Manuscript prepared for J. Name
with version 2015/09/17 7.94 Copernicus papers of the LaTeX class copernicus.cls.
Date: 14 June 2017

Response to Editor

'Open-source sea ice drift algorithm for Sentinel-1 SAR imagery using a combination of feature-tracking and pattern-matching'

Stefan Muckenhuber and Stein Sandven
Nansen Environmental and Remote Sensing Center (NERSC), Thormøhlensgate 47,
5006 Bergen, Norway
Correspondence to: S. Muckenhuber (stefan.muckenhuber@nersc.no)

Dear Professor Lars Kaleschke,

Thank you very much for helping us improving our paper.

Please find here the **answers** to your comments:

1 Comment from the editor

The manuscript requires still further improvements before it can be accepted. In addition to the comments raised by the referee I'd like to stress that the quality of the presentation is still not yet satisfying. As already stated previously, the vectors in Fig. 3 are largely overlapping, Fig. 5 and 7 have no axis labels and the meaning and significance is not clear.

To avoid the large vector overlaps in Figure 3 (now Figure 4), we zoomed into a smaller part of the image pair and depict the coverage of the corresponding zoomed area and of the entire image pair Fram Strait in an additional plot (Figure 1). We changed and added the captions according to this adjustment.

We added axis labels to Figure 5 and 7 (now Figure 6 and 8) and changed the captions accordingly. We believe that Figure 5 and 7 are essential to understand the algorithm and in particular to understand the python code. The two figures depict the matrices that are used in the algorithm code and show how the algorithm creates and handles the first guess as well as the distance d distribution. We hope that by adding axis labels and the following sentences, the meaning and significance of the two figures will become more clear:

(this figure illustrates the matrices that the algorithm considers as first guess)

The figure depicts the matrix that the algorithm considers for the distribution of d.

A section of "author contributions" is missing.

We added the following section:

Author contributions. Stefan Muckenhuber designed the algorithm and the experiments, performed the data analysis and interpretation of the results and wrote the manuscript. Stein Sandven critically revised the work and gave important feedback for improvement. Stefan Muckenhuber and Stein Sandven approved the final version for publication.

I further highly recommended to obtain a DOI for the code in the Github repository. Otherwise it is not clear to which version you refer to.

Due to the recent rivalling publication, we do not dare to distribute the recent version of our code before the final publication of this manuscript. However, we will add the algorithm including an application example as supplement to this manuscript. This way, the DOI of the manuscript will refer to both the manuscript and the code. We changed the last sentence in Section 'Open-source distribution' to:

The presented sea ice drift algorithm, including an application example, is distributed as open-source software as supplement to this manuscript.

Please find attached the corrected manuscript with changes marked in blue and red.

Thanks again for your comments. We are looking forward to your reply!

Best regards,

S. Muckenhuber and S. Sandven

Manuscript prepared for J. Name
with version 2015/09/17 7.94 Copernicus papers of the LaTeX class copernicus.cls.
Date: 14 June 2017

Response to Referee # 1

'Open-source sea ice drift algorithm for Sentinel-1 SAR imagery using a combination of feature-tracking and pattern-matching'

Stefan Muckenhuber and Stein Sandven

Nansen Environmental and Remote Sensing Center (NERSC), Thormøhlensgate 47,
5006 Bergen, Norway

Correspondence to: S. Muckenhuber (stefan.muckenhuber@nersc.no)

Dear Referee # 1,

Thank you very much for helping us improving our paper.

Please find here the **answers** to your comments and the corresponding ***changes in manuscript***:

1 Introduction

Thank you for your detailed reply to my comments and the significant improvements in your paper. It is nice to see this tempting idea evolving and over all the paper is now worth being publishing after some more revisions to be done. The only fundamental problem I see is the parallel publication on the same topic from two other authors (actually two research group leaders!) from the same institute but this should not be a problem of an individual PhD student especially since the this respective discussion paper by Muckenhuber and Sandven has been published earlier and the associated code has been made publically available. At the end, it is a decision only the editorial board of the Cryosphere can make.

We agree that this has been a very unfortunate development and we are happy that the editor acknowledges that our manuscript was submitted earlier and published first in The Cryosphere Discussion. In the future we will avoid the distribution of any unpublished material if not absolutely necessary.

This having said, I'm afraid that I have still some comments. During the last revisions I asked to be more careful regarding some claims by asking for "softer" phrases and adding a more detailed analysis. The three main claims of the paper are:

1. The authors use feature tracking for a first guess to be computational more efficient than pure pattern matching

2. The first guess is based on independent vectors - therefore the authors are more capable to resolve deformation zones

3. HV polarization is better for feature tracking and therefore potentially as well for pattern matching

4. The algorithm can handle rotation

It is obvious that the setup of the algorithm allows a better handling of rotation but it is less obvious and not shown in the paper, that the algorithm is actually faster than pure pattern matching algorithms, that they can handle deformations and shear regions in a better way or that the use of HV data is more advantageous for pattern matching as well (see as well my thought in the last review which the authors included in the paper as well). I won't say that these claims are not potentially true but the authors neither show nor prove it. It's merely a question of the wording and no extra science that needs to be done but the first three claims are not as obvious as the authors suggest. (e.g. it might be better to say that the first guess by feature tracking potentially allows a computational efficient computation than claiming that it is more efficient that pure pattern matching. If you want to claim it: prove it!). It might not sound that sexy but it would be more precise. The same holds true for claim 2 and 3.

We agree that there are certainly pattern-matching approaches that are computationally more efficient than the presented combined approach and we did not anticipate to claim that our feature-tracking algorithm is faster than all pattern-matching methods. We rather wanted to introduce a new approach that combines the advantages of the considered feature-tracking method and the considered (simple) pattern-matching method. We tried to rephrase the manuscript according to that.

We did not want to claim that our algorithm is more capable to resolve shear and deformation zones than all pattern-matching approaches, but rather wanted to mention that the independence of the feature-tracking vectors in terms of position, lengths, direction and rotation can potentially be an important advantage for resolving shear zones, rotation and divergence/convergence zones. We also mention that the feature-tracking approach might miss shear and convergence/divergence zones due to the uneven vector coverage. We rephrased the following sentence accordingly:

This can be done computationally efficient and the resulting vectors are often independent of their neighbours in terms of position, lengths, direction and rotation, which can potentially be an important advantage for resolving shear zones, rotation and divergence/convergence zones.

We believe that the considered feature-tracking approach performs better using HV polarisation. However, we agree that this does not mean that HV is the better approach for pattern-matching (or any other type of feature-tracking). It was not our intention to claim that. This was expressed in the Discussion with the sentence 'However, at this point, these are

just assumptions and will be addressed in more detail in our future work.' We also mentioned that HH could be the better channel for pattern-matching. We tried to further remove phrases that could lead to this misunderstanding and changed among others the following sentence:
And more consistent features could potentially also favour the performance of the pattern-matching step, but this is only an assumption and has not been tested yet.

One last thing before I deal with the comments in detail: Personally I think that the authors stress the computational efficiency of their algorithm a bit too much and avoid every operation that could hamper this goal. That's okay but it should be discussed in the text (e.g. "a better way to determine d would be to take into account the variability of the vectors as well we avoided it for the sake of computational efficiency") In this way the readers would be aware of these limitations. Just scan through your last answers to my comments for the term computational efficiency and add some explanation at the respective position in the manuscript. Besides that the DTU shows that operational products a possible with pure pattern matching as well.

We aim to deliver an open-source algorithm that is computationally efficient enough that a relatively high number of image pairs can be processed without the need for an expensive server or super-computing facility. This way a higher number of stackholder shall be reached and the possibility for computing sea ice drift on a standard PC shall be created for everyone. Therefore, the computational efficiency of the presented algorithm has a high priority for us. It is true that DTU provides an operational product based on pure pattern-matching. However the considered resolution is in the order of 10 km and the algorithm is not open source, which also means that we don't know the computational efficiency. We scanned through the last comments and added the following explanations:
For the sake of computational efficiency, the same intensity value scaling is used for the pattern-matching step.
For the sake of computational efficiency, the vectors from all resolution pyramid levels are treated equally.
(NB: the representativeness also depends on the variability of the surrounding vectors, but for the sake of computational efficiency, we only consider the distance d as representativeness measure)
As an alternative, one could adjust the search window according to the time span. However, this would add additional complexity to both the algorithm and the parameter evaluation and needs more research on how the search window should be adjusted depending on the time span. For the sake of computational efficiency, we suggest the simple approach to remove final drift vectors above the maximum speed.

2 Comments on Response to Referee #1

The authors answered most of my questions and solved many of the problems I mentioned. Thanks for that. In the following I will focus on the points only, where I do not agree with the answers which thereby might sound more negative than actually meant.

Page 1 Line 14ff the authors are of course right that the noise level depends on the incident angle. However, there is a pattern of the noise level (e.g. https://doi.org/10.1016/j.procs.2016.09.247 and ESA mentions -25 dB and -22 dB). But if the authors basically use a fixed threshold for the scaling of all scenes, I would like to ask for a reference that suggests doing so or containing information about the variation of noise level over the swath width. It might hold true for some scenes but definitely not for all and would lead to a scaling over a value range containing only e.g. 50% meaning full values or throw away 50% of values containing information in the case the authors showed and used to make the point that there approach is correct . But if the distribution has so many values in in the range below the noise level it is at least worth checking if the calibration routines of Nansat work properly (the scaling itself provides somehow has to provide a reasonable image otherwise, there would not be any data.

We agree that there are several different noise pattern in the SAR data, but for the sake of simplicity we use fixed thresholds for the scaling. The reference that suggested using the applied thresholds for the feature-tracking approach is Muckenhuber et al. (2016). Muckenhuber et al. (2016) tuned the brightness boundaries to achieve the highest number of vectors and we want to build on this experience, rather than concentrating on a new pre-processing procedure. Angular dependent pre-processing for HH and thermal noise correction for HV has certainly the potential to improve the results significantly and we are looking forward to apply upcoming procedures for our algorithm. For this manuscript however, it is not our main goal to find the best possible pre-processing procedure, since there are other more qualified people working on this topic and we want to concentrate on the algorithm steps after the pre-processing. We checked the calibration routines of Nansat, discussed the topic with people at TU Wien and JPL and did not find any mistakes so far. We included Figure 3 that shows the images with the intensity values and range that we use in the algorithm. The figure has been produced using the presented pre-processing and therefore represents the input matrix for the feature-tracking and pattern-matching step. Most of the values above our considered brightness threshold are over land and therefore not of interest for us. Some low incidence angle HH values over sea ice might have been excluded, but we believe that this is a reasonable compromise for applying a simple (and computationally efficient) pre-processing to which we already have a parameter suggestion from Muckenhuber et al. (2016).

Page 2 Line 40 "... an even better parameter set, because a higher number Is considered ..." It is not the same, it is a completely different approach and therefore not better but just different, providing different information but I'm okay with it.

We agree that this is only a different but not necessarily better approach.

Page 2 Line 50 "... more feature tracking vectors are found on image pair with a smaller time span" - given a sufficient number of linear features visible in HV, only and not in the less textures areas where the feature tracking algorithm tends to fail I would like to add but as I said, I guess, that's okay.

We agree. This only holds in areas where a sufficient number of corners are detected by the feature-tracking algorithm.

Page 3 Line 80: I understand the point of the authors and agree with them! Having said this, I'm not happy with it and don't think that things like this should happen since it is bad science and from an outside perspective creates the impression that NERSC has more expertise in the field of sea ice drift than there is actually available plus increases the noise level for publications in this field in general, which makes it more difficult to keep an overview of relevant publications. However, as I stated in my introduction it is up to the editorial board of the Cryosphere to decide.

We agree and we are also very unhappy with this development. We will stronger protect our unpublished work in the future.

Page 4 Line 93: The mentioned independence is not only reduced by overlapping / close features but as well by very characteristic and bright features that might be represented in all resolution levels of the ORB algorithm but I guess that's okay

We agree that the independence is also reduced by features that are detected in more than one resolution pyramid. We meant to include those features in the phrase 'overlapping'. Defining not only the corner, but the area around the corner (considered by the descriptor) as 'feature', the features from different resolution levels are usually overlapping too.

Page 4 Line 105: The feature tracking algorithm chooses the best detectable features automatically but this means that there can also be vast areas with no feature tracking vectors at all if there are enough well defined ridges is one corner of the scene. For the first guess the motion field is now interpolated over these vast "vector"-less areas as well. I have my doubts if this is better or more independent than a fine tuned resolution pyramid in the case of pattern matching. I suggest skipping this comparative statement

We agree. There has been no comparison or proof that would support this sentence. This sentence is rather an idea or motivation for us to follow this new approach than a proven

statement and should therefore be skipped. A well tuned pattern-matching approach has certainly the potential to outperform the presented combined algorithm.

Page 5 Line 134 f It is not necessarily true that a scaling that favours feature tracking favours pattern matching as well. 1. The NCC needs no scaling at all since it is normalized (the N of NCC) and 2. Imagine an extreme scaling that would separate ridges in white from the surrounding background in black. For feature tracking, this would be perfect, since it would highlight the linear feature. For pattern matching it would be a problem, especially in the regions outside the ridged areas since it is based on areal pattern variation.

We agree that the scaling that favours our feature-tracking approach not necessarily favours the considered pattern-matching method. Nevertheless, for the sake of simplicity and computational efficiency, we would like to use the same image matrix for both feature-tracking and pattern-matching. This is now also mentioned in the sentence:

For the sake of computational efficiency, the same intensity value scaling is used for the pattern-matching step.

Page 8 Line 242 Thanks for the explanation. Just mention it in the manuscript

We added the following to the manuscript:

Sea ice drift might be different on different resolution scales. This is particularly an issue in the case of rotation. The feature-tracking vectors provide the first guess and this vector field should represent the same drift resolution as considered by the pattern-matching step.

Page 9 Line 291 "We believe ... " I suggest to show it or be more careful with such a statement. The ice drift of the e.g. for example is pure pattern matching without any fancy resolution pyramid and runs pretty fast to provide the ice drift within the framework of CMEMS.

We agree. There are certainly very reliable pattern-matching procedures that can outperform our combined approach in terms of computational effort, independence and rotation. We were focusing too much on the simple pattern-matching procedure that we implemented as part of this algorithm and wanted to highlight the potential advantages of the combined algorithm rather than claiming a real comparison with existing and well tuned pure pattern-matching procedures. This paragraph should be skipped.

Page 12 Line 409 / Page 13 Line 437 the authors promise to bring feature tracking performance of HH closer to HV by an increased coverage of S1 images and a better pre-processing. I would claim that HH and HV show different characteristics and that's it. You won't change the stronger dependency of linear features in HH polarised images from the incident angle by increasing the

temporal resolution but may see other features. Having said this, a better pre-processing and a higher temporal resolution never hurts and will improve the results for sure.

We agree that HH and HV show different characteristics and that alone could explain the difference in feature-tracking performance. Muckenhuber et al. (2016) found the best HH performance on the image pair with shortest time gap. Since they compared only four image pairs (from different regions), this could certainly be an coincidence. But it could also potentially mean that HH features are more likely to be destroyed over time. However, this is only an assumption and since the data is not sufficient, we don't want to claim it. We rather wanted to introduce the idea.

3 The Manuscript itself

Most of the remaining points I already handled in my answers to your comments, meaning there is not much left.

3.1 Still open points from previous reviews

Page 4 Line 119 f - see as well my comment above: the independence is difficult to assess and its effect on resolving deformation zones is not shown in this paper - may be more careful

We agree that the general comparison of feature-tracking and pattern-matching in terms of vector independence and effects on resolving shear zones is very difficult and has not been done here. We rather wanted to highlight the characteristics of the considered feature-tracking method and the considered pattern-matching method and tried to rephrase the manuscript accordingly. See also the answer to the comment above.

Page 7 Line 210 - 215 See my comment to your answers

See answer to first comment in Comments on Response to Referee #1

Page 16 Line 393 I think we had this discussion already in the first draft. I think it is difficult to use a buoy dataset for validation if you used the same dataset beforehand to optimise the setup of the algorithm (Page 16 Line 370-377). It does not result in a real assessment of the performance of the algorithm but in the potentially performance in the case that the algorithm is tuned in the right way to the respective ice conditions.

Rather than optimising or tuning the algorithm, we wanted to find search restrictions for the search area t_{2s} and rotation β that are reasonable for our area and time period. We understand your concerns regarding this and tried to rephrase the manuscript accordingly. We changed the following sentences:

To assess the potential performance after finding suitable search restrictions, calculated drift

results from 246 Sentinel-1 image pairs have been compared to buoy GPS data, collected in 2015 between 15th January and 22nd April and covering an area from 80.5° N to 83.5° N and 12° E to 27° E. We found a logarithmic normal distribution of the displacement difference with a median at 352.9 m using HV polarisation and 535.7 m using HH polarisation.

The algorithm description including data pre-processing is given in Section 3, together with tuning and performance assessment methods. Section 4 presents the pre-processing, parameter tuning and performance assessment results and provides a recommended parameter setting for the area and time period of interest.

To evaluate suitable search limitations and assess the potential algorithm performance, we use GPS data from drift buoys that have been set out in the ice covered waters north of Svalbard as part of the Norwegian Young Sea Ice Cruise (N-ICE2015) project of the Norwegian Polar Institute (Spreen and Itkin, 2015).

Performance assessment

Using the recommended search restrictions from above, the algorithm has been compared to the N-ICE2015 GPS buoy data set (Figure 9) to assess the potential performance after finding suitable search restrictions for the area and time period of interest.

The results of the conducted performance assessment are shown in Figure 12.

The conducted performance assessment also reveals a logarithmic normal distribution of the distance D (Equation 15) that can be expressed by the following probability density function (solid red line in Figure 12):

Based on the restriction evaluation, our experience with the algorithm behaviour, and considering a good compromise between computational efficiency and high quality of the resulting vector field, we recommend the parameter setting shown in Table 1 for our area and time period of interest.

To estimate the potential performance of the introduced algorithm for given image pairs, given ice conditions, given region and given time, we compared drift results from 246 Sentinel-1 image pairs with corresponding GPS positions from the N-ICE2015 buoy data set.

3.2 Technical comments

Page 3 Line 62: "On the one hand... on the other hand" - there is "the one hand" missing

We agree and changed the sentence to:

Unlike optical sensors, Space-borne Synthetic Aperture Radar (SAR) are active sensors, operate in the microwave spectrum and can produce high resolution images regardless of solar illumination and cloud cover.

Page 4 Line 105 since you mention in line 104 that the area has a revisit time of less than one day it is obvious that your area of interest is monitored on a daily basis

We agree and changed the sentence to:

The sea ice covered oceans in the European Arctic Sector represent an important area of interest for the Sentinel-1 mission and due to the short revisit time in the Arctic, our area of interest is monitored by Sentinel-1 on a daily basis (ESA, 2012).

Page 13 Line 324 "accurate drift" - it not necessary a more accurate drift but merely a more localised/ locally tuned/ locally adapted one. The term "accurate" sounds good but has a meaning which has nothing to do with the case at hand - nevertheless we might hope that a locally adapted drift vector represents the drift at a certain position more accurately than the first guess but that is not necessarily the case.

We agree and changed the sentence to:

We apply pattern-matching at chosen points of interest to adjust the drift and rotation estimate at these specific locations.

Page 15 Lin 363 "since the uncertainty increases with distance d (Figure 7)" - may be rephrase the sentence - the authors are correct but it suggests that Figure 7 shows the increase of "uncertainty" depending on the distance. Having said this: "uncertainty" is a statistical term - may be choose something less well defined.

We agree and changed the sentence to:

Since the representativeness of the first guess decreases with distance d ***to the closest feature-tracking vector (an example to illustrate the distribution of*** d ***is shown Figure 8), the search restrictions*** t_{2s} ***and*** β ***should increase with*** d***.***

Page 15 Line 368 / Page 17 Line 405 - it is more or less the same sentence, may be skip one

We skipped the sentence on page 15 Line 368 and changed the following sentence to:

Based on the performed search restriction evaluation (Section 4), we found the following functions to represent useful restrictions for our area and time period of interest.

Page 21 Line 482 "accuracy of the introduced algorithm" I suggest to add "for given image pairs, given ice conditions, given region and given time" since the results are not transferable to other ice conditions or regions...

We agree and changed the sentence to:

To estimate the potential performance of the introduced algorithm for given image pairs, given ice conditions, given region and given time, we compared drift results from 246 Sentinel-1 image

pairs with corresponding GPS positions from the N-ICE2015 buoy data set.

Please find attached the corrected manuscript with changes marked in blue and red.

Thanks again for your comments. We are looking forward to your reply!

Best regards,

S. Muckenhuber and S. Sandven

Manuscript prepared for J. Name
with version 2015/09/17 7.94 Copernicus papers of the LaTeX class copernicus.cls.
Date: 14 June 2017

Open-source sea ice drift algorithm for Sentinel-1 SAR imagery using a combination of feature-tracking and pattern-matching

Stefan Muckenhuber and Stein Sandven

Nansen Environmental and Remote Sensing Center (NERSC), Thormøhlensgate 47,
5006 Bergen, Norway

Correspondence to: S. Muckenhuber (stefan.muckenhuber@nersc.no)

Abstract. An open-source sea ice drift algorithm for Sentinel-1 SAR imagery is introduced based on the combination of feature-tracking and pattern-matching. Feature-tracking produces an initial drift estimate and limits the search area for the consecutive pattern-matching, that provides small to medium scale drift adjustments and normalised cross-correlation values. The algorithm is designed to combine the two approaches in order to benefit from the respective advantages. The ~~main advantages of the~~ considered feature-tracking ~~approach are the computational efficiency and the independence of the vectors~~ method allows a computationally efficient computation of the drift field and the resulting vectors show a high degree of independence in terms of position, lengths, direction and rotation. ~~Pattern-matching~~ The considered pattern-matching method on the other side allows better control over vector positioning and resolution. The pre-processing of the Sentinel-1 data has been adjusted to retrieve a feature distribution that depends less on SAR backscatter peak values. Applying the algorithm with the recommended parameter setting, sea ice drift retrieval with a vector spacing of 4 km on Sentinel-1 images covering 400 km x 400 km, takes about 4 minutes on a standard 2.7 GHz processor with 8 GB memory. The corresponding recommended patch size for the pattern-matching step, that defines the final resolution of each drift vector is 34×34 pixels (2.7×2.7 km). ~~For validation~~To assess the potential performance after finding suitable search restrictions, calculated drift results from 246 Sentinel-1 image pairs have been compared to buoy GPS data, collected in 2015 between 15^{th} January and 22^{nd} April and covering an area from 80.5° N to 83.5° N and 12° E to 27° E. We found a logarithmic normal distribution of the ~~error~~ displacement difference with a median at 352.9 m using HV polarisation and 535.7 m using HH polarisation. All software requirements necessary for applying the presented sea ice drift algorithm are open-source to ensure free implementation and easy distribution.

1 Introduction

Sea ice drift has a strong impact on sea ice distribution on different temporal and spatial scales. Motion of sea ice due to wind and ocean currents causes convergence and divergence zones, resulting in formation of ridges and opening/closing of leads. On large scales, ice export from the Arctic and Antarctic into lower latitudes, where the ice eventually melts away, contributes to a strong seasonality of total sea ice coverage (IPCC, 2013). Due to a lack of ground stations in sea ice covered areas, satellite remote sensing represents the most important tool for observing sea ice conditions on medium to large scales. Despite the strong impact of sea ice drift and the opportunities given by latest satellite remote sensing techniques, there is a lack of extensive ice drift data sets providing sufficient resolution for estimating sea ice deformation on a spatial scaling of less than 5 km.

Our main regions of interest are the ice covered seas around Svalbard and East of Greenland. Characteristic for this area are a large variation of different ice types (Marginal Ice Zone, First Year Ice, Multi Year Ice etc.), a strong seasonality of ice cover and a wide range of drift velocities. Focus was put on the winter/spring period, since the area of interest experiences the highest ice cover during this time of the year.

Early work from Nansen (1902) established the rule-of-thumb that sea ice velocity resembles 2 % of the surface wind speed with a drift direction of about 45° to the right (Northern Hemisphere) of the wind. This wind driven explanation can give a rough estimate for instantaneous ice velocities. However, the respective influence of wind and ocean current strongly depends on the temporal and spatial scale. Only about 50 % of the long-term (several months) averaged ice drift in the Arctic can be explained by geostrophic winds, whereas the rest is related to mean ocean circulation. This proportion increases to more than 70 % explained by wind, when considering shorter time scales (days to weeks). The wind fails to explain large-scale ice divergence patterns and its influence decreases towards the coast (Thorndike and Colony, 1982).

Using GPS drift data from the International Arctic Buoy Program (IABP), Rampal et al. (2009) analysed the general circulation of the Arctic sea ice velocity field and found that the fluctuations follow the same diffusive regime as turbulent flows in other geophysical fluids. The monthly mean drift using 12 h displacements was found to be in the order of 0.05 to 0.1 m/s and showed a strong seasonal cycle with minimum in April and maximum in October. The IABP dataset also revealed a positive trend in the mean Arctic sea ice speed of +17 % per decade for winter and +8.5 % for summer considering the time period 1979–2007. This is unlikely to be the consequence of increased external forcing. Instead, the thinning of the ice cover is suggested to decrease the mechanical strength which eventually causes higher speed given a constant external forcing (Rampal et al. , 2009b).

Fram Strait represents the main gate for Arctic ice export and high drift velocities are generally found in this area with direction southward. Based on moored Doppler Current Meters mounted near 79° N 5° W, Widell et al. (2003) found an average southward velocity of 0.16 m/s for the period

1996–2000. Daily averaged values were usually in the range 0–0.5 m/s with very few occasions above 0.5 m/s.

GPS buoys and Current Meters are important tools to measure ice drift at specific locations. However, to monitor sea ice drift on medium to large scales, satellite remote sensing represents the most important data source today. The polar night and a high probability for cloud cover over sea ice limit the capability of optical sensors for reliable year-round sea ice monitoring. Unlike optical sensors, Space-borne Synthetic Aperture Radar (SAR) ~~, on the other hand, are active microwave sensors~~are active sensors, operate in the microwave spectrum and can produce high resolution images regardless of solar illumination and cloud cover. Since the early 1990's SAR sensors are delivering systematic acquisitions of sea ice covered oceans and Kwok et al. (1990) showed that sea ice displacement can be calculated from consecutive SAR scenes.

The geophysical processor system from Kwok et al. (1990) has been used to calculate sea ice drift fields in particular over the Western Arctic (depending on SAR coverage) once per week with a spatial resolution of 10-25 km for the time period 1996–2012. This extensive dataset makes use of SAR data from RADARSAT-1 operated by the Canadian Space Agency, and from ENVISAT (Environmental Satellite) ASAR (Advanced Synthetic Aperture Radar) operated by ESA (European Space Agency).

To resolve drift details on a finer scale, a high-resolution sea ice drift algorithm for SAR images from ERS-1 (European Remote-sensing Satellite from ESA) based on pattern-matching was introduced by Thomas et al. (2008), that allowed drift calculation with up to 400 m resolution. Hollands and Dierking (2011) implemented their own modified version of this algorithm to derive sea ice drift from ENVISAT ASAR data.

To provide drift estimates also in areas where areal matching procedures (like cross and phase correlation) fail, Berg and Eriksson (2014) introduced a hybrid algorithm for sea ice drift retrieval from ENVISAT ASAR data using phase correlation and a feature based matching procedure that is activated if the phase correlation value is below a certain threshold.

The current generation of SAR satellites including RADARSAT-2 and Sentinel-1 are able to provide images with more than one polarisation. Komarov and Barber (2014) and Muckenhuber et al. (2016) have evaluated the sea ice drift retrieval performance with respect to the polarisation using a combination of phase/cross-correlation and feature-tracking based on corner detection respectively. Muckenhuber et al. (2016) has shown that feature-tracking provides on average around four times as many vectors using HV polarisation compared to HH polarisation.

After the successful start of the Sentinel-1 mission in early 2014, high-resolution SAR images are delivered for the first time in history within a few hours after acquisition as open-source data to all users. This introduced a new era in SAR Earth observation with great benefits for both scientists and other stack holders. Easy, free and fast access to satellite imagery facilitate the possibility to provide products on an operational basis. The Danish Technical University (Pedersen et al.

(2015), http://www.seaice.dk/) provides an operational sea ice drift product based on Sentinel-1 data with 10 km resolution as part of the Copernicus Marine Environment Monitoring Service (CMEMS, http://marine.copernicus.eu).

The sea ice covered oceans in the European Arctic Sector represent an important area of interest for the Sentinel-1 mission and ~~with having a revisit time of less than one day~~ due to the short revisit time in the Arctic~~(ESA, 2012)~~, our area of interest is monitored by Sentinel-1 on a daily basis (ESA, 2012).

This paper follows up the work from Muckenhuber et al. (2016), who published an open-source feature-tracking algorithm to derive computationally efficient sea ice drift from Sentinel-1 data based on the open-source ORB algorithm from Rublee et al. (2011), that is included in the OpenCV Python package. We aim to improve the feature-tracking approach by combining it with pattern-matching. Unlike Berg and Eriksson (2014), the feature-tracking step is performed initially and serves as a first guess to limit the ~~computational effort~~ search area of the pattern-matching step.

From a methodological point of view, algorithms for deriving displacement vectors between two consecutive SAR images are based either on feature-tracking or pattern-matching.

Feature-tracking detects distinct patterns (features) in both images and tries to connect similar features in a second step without the need for knowing the locations. This can be done computationally efficient and the resulting vectors are often independent of their neighbours in terms of position, lengths, direction and rotation, which ~~is~~ can potentially be an important advantage for resolving shear zones, rotation and divergence/convergence zones. The considered feature-tracking approach identifies features without taking the position of other features into account and matches features from one image to the other without taking the drift and rotation information from surrounding vectors into account (Muckenhuber et al., 2016). However, due to the independent positioning of the features, very close features may share some pixels and since all vectors from the resolution pyramid are combined, the feature size varies among the matches, which implies a varying resolution. In addition, the resulting vector field is not evenly distributed in space and large gaps may occur between densely covered areas, which can eventually lead to missing a shear or divergence/convergence zone.

Pattern-matching, on the other hand, takes a small template from the first image at the starting location of the vector and tries to find a match on a larger template from the second image. ~~Despite~~ Simple pattern-matching methods based on normalised cross-correlation often demand a considerable computational effort. Nevertheless, this approach is widely used, since it allows to define the vector positions. For practical reasons, a pyramid approach is generally used to derive high-resolution ice drift. This speeds up the processing, but potentially limits the independence of neighbouring vectors, since they depend on a lower resolution estimate (Thomas et al., 2008).

The objective of this paper is to combine the two approaches in order to benefit from the respective advantages. The main advantages of the considered feature-tracking approach are the computational efficiency and the independence of the vectors in terms of position, lengths, direction and rotation.

~~Pattern-matching~~ The considered pattern-matching method on the other side allows better control over vector positioning and resolution, which is a necessity for computing divergence, shear and total deformation.

The presented algorithm, all necessary software requirements (python incl. Nansat, openCV and SciPy) and the satellite data from Sentinel-1 are open-source. A free and user friendly implementation shall support an easy distribution of the algorithm among scientists and other stakeholders.

The paper is organised as follows: The used satellite products and buoy data are introduced in Section 2. The algorithm description including data pre-processing is given in Section 3, together with tuning and ~~validation~~ performance assessment methods. Section 4 presents the pre-processing, parameter tuning and ~~validation~~ performance assessment results and provides a recommended parameter setting for the area and time period of interest. The discussion including outlook can be found in Section 5.

2 Data

The Sentinel-1 mission is a joint initiative of the European Commission and the European Space Agency (ESA) and represents the Radar Observatory for the Copernicus Programme, a European system for monitoring the Earth with respect to environmental and security issues. The mission includes two identical satellites, Sentinel-1A (launched in April 2014) and Sentinel-1B (launched in April 2016), each carrying a single C-band SAR with a centre frequency of 5.405 GHz and dual-polarisation support (HH+HV, VV+VH) also for wide swath mode. Both satellites fly in the same near-polar, sun-synchronous orbit and the revisit time is less than 1 day in the Arctic (ESA, 2012). The main acquisition mode of Sentinel-1 over sea ice covered areas is Extra Wide Swath Mode Ground Range Detected with Medium Resolution (EW GRDM) and the presented algorithm is built for processing this data type. The covered area per image is 400 km $\times$ 400 km and the data are provided with a pixel spacing of 40 m $\times$ 40 m in both HV and HH polarisation. The introduced algorithm can utilise both HV and HH channel. However, the focus of this paper is put on using HV polarisation (mainly acquired over the European Arctic and the Baltic sea), since this channel provides in our area of interest on average four times more feature tracking vectors than HH (Muckenhuber et al., 2016), representing a better initial drift estimate for the combined algorithm.

To illustrate the algorithm performance and explain the individual steps, we use an image pair acquired over Fram Strait. The acquisition times of the two consecutive images are 2015-03-28 07:44:33 (UTC) and 2015-03-29 16:34:52 (UTC), and the covered area is shown in Figure ~~4~~1. This image pair covers a wide range of different ice conditions (multiyear ice, first-year ice, marginal ice zone etc.) and the ice situation is representative for our area and time period of interest.

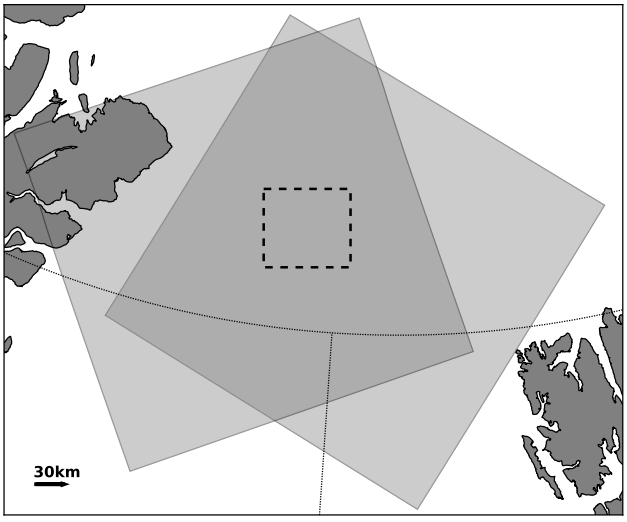

Figure 1. Coverage of image pair Fram Strait that is used as representative image pair to explain the algorithm approach. The dashed rectangle depicts the area shown in Figure 4 to illustrate the vector distribution of the algorithm steps.

To evaluate suitable search limitations and ~~validate the algorithm~~assess the potential algorithm performance, we use GPS data from drift buoys that have been set out in the ice covered waters north of Svalbard as part of the Norwegian Young Sea Ice Cruise (N-ICE2015) project of the Norwegian Polar Institute (Spreen and Itkin, 2015). The ice conditions during the N-ICE2015 expedition are describe on the project website (http://www.npolar.no/en/projects/n-ice2015.html) as challenging. The observed ice pack, mainly consisting of 1.3-1.5 m thick multiyear and first-year ice, drifted faster than expected and was very dynamic. Closer to the ice edge, break up of ice floes has been observed due to rapid ice drift and the research camp had to be evacuated and re-established four times. This represents a good study field, since these challenging conditions are expected in our area and time period of interest. The considered GPS data have been collected in 2015 between 15^{th} January and 22^{nd} April, and cover an area ranging from 80.5° N to 83.5° N and 12° E to 27° E. The buoys recorded their positions either hourly or every three hours. In the later case, the positions have been interpolated for each hour.

3 Method

3.1 Data pre-processing

To process Sentinel-1 images within Python (extraction of backscatter values and corresponding geolocations, reprojection, resolution reduction etc.), we use the Python toolbox Nansat (Korosov et al., 2016), that builds on the Geospatial Data Abstraction Library (http://www.gdal.org). As done

in Muckenhuber et al. (2016), we change the projection of the the provided ground control points (latitude/longitude values given for certain pixel/line coordinates) to stereographic and use spline interpolation to calculate geographic coordinates. This provides a good geolocation accuracy also at high latitudes. The pixel spacing of the image is changed by averaging from 40 m to 80 m, which is closer to the sensor resolution of 93 m range × 87 m azimuth, and decreases the computational effort.

For each pixel p, the Sentinel-1 data file provides a digital number DN_p and a normalisation coefficient A_p, from which the normalised radar cross section σ^0_{raw} is derived by the following equation:

$$\sigma^0_{\text{raw}} = DN_p^2 / A_p^2 \tag{1}$$

The normalised radar cross section σ^0_{raw} reveals a logarithmic distribution and the structures in the sea ice are mainly represented in the low and medium backscatter values rather than in the highlights. Therefore, we change the linear scaling of the raw backscatter values σ^0_{raw} to a logarithmic scaling and get the backscatter values $\sigma^0 = 10 * \lg(\sigma^0_{\text{raw}})$ [dB]. A representative backscatter distribution over sea ice is shown in Figure 2. Using a logarithmic scaling provides a keypoint distribution for the feature tracking algorithm that depends less on high peak values, while the total number of vectors increases.

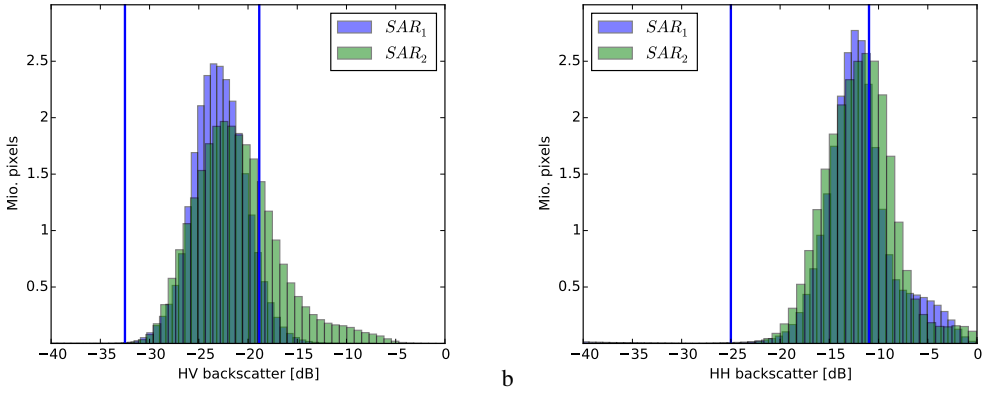

Figure 2. Histogram of (a) HV and (b) HH backscatter values σ^0 from image pair Fram Strait. The lower and upper brightness boundaries for HV ($\sigma^0_{\text{min}} = -32.5$ dB, $\sigma^0_{\text{max}} = -18.86$ dB) and HH ($\sigma^0_{\text{min}} = -25.0$ dB, $\sigma^0_{\text{max}} = -10.97$ dB) are shown with blue lines and illustrate the domain for the intensity values i.

To apply the feature-tracking algorithm from Muckenhuber et al. (2016), the SAR backscatter values σ^0 have to be converted into intensity values i with $0 \leq i \leq 255$ for $i \in \mathbb{R}$. This conversion is done by using Eq. (2) and setting all values outside the domain to 0 and 255.

$$i = 255 \cdot \frac{\sigma^0 - \sigma^0_{\text{min}}}{\sigma^0_{\text{max}} - \sigma^0_{\text{min}}} \tag{2}$$

The upper brightness boundary σ^0_{max} is set according to the recommended value from Muckenhuber et al. (2016), i.e. -18.86 dB and -10.97 dB for HV and HH respectively. The lower boundary σ^0_{min} was chosen to be -32.5 dB (HV) and -25.0 dB (HH), since this was found to be a reasonable range of expected backscatter values. Figure 3 shows the image pair Fram Strait after the conversion into intensity values. For the sake of computational efficiency, the same intensity value scaling is used for the pattern-matching step.

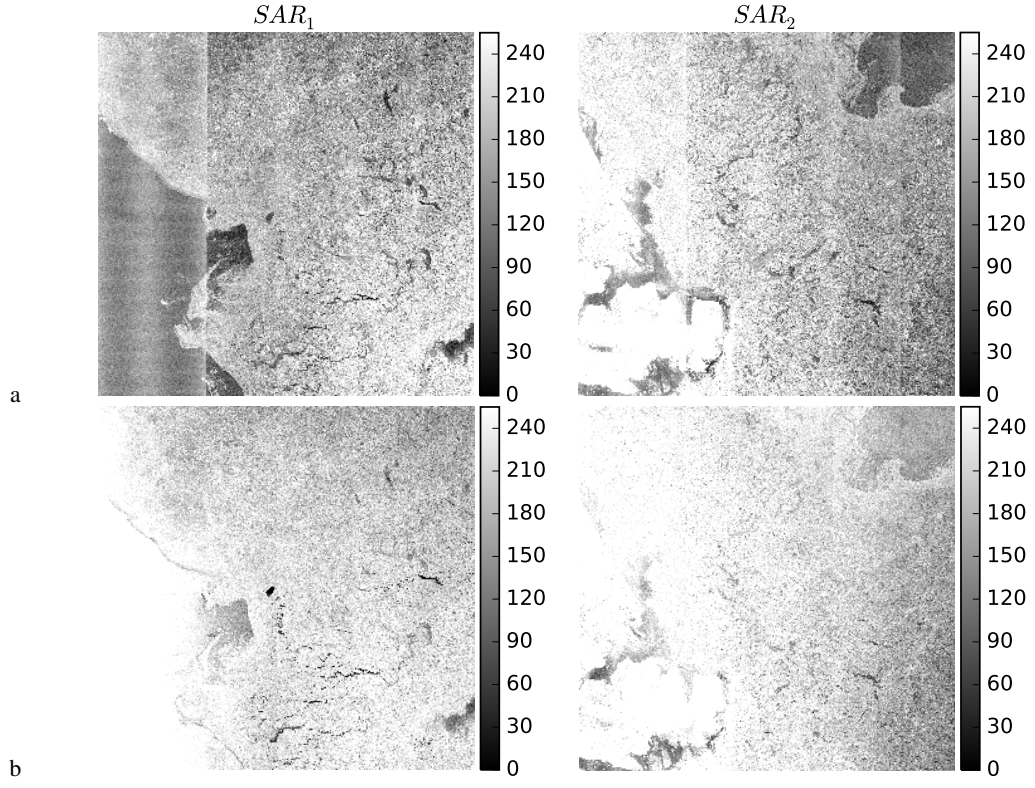

Figure 3. Image pair Fram Strait in (a) HV and (b) HH polarisation after conversion (Equation 2) from backscatter values σ^0 into intensity values with range $0 \leq i \leq 255$ using lower and upper brightness boundaries for HV: $\sigma^0_{\text{min}} = -32.5\,\text{dB}$ and $\sigma^0_{\text{max}} = -18.86\,\text{dB}$ and HH: $\sigma^0_{\text{min}} = -25.0\,\text{dB}$, $\sigma^0_{\text{max}} = -10.97\,\text{dB}$.

3.2 Sea ice drift algorithm

The presented sea ice drift algorithm is based on a combination of feature-tracking and pattern-matching, and is designed to utilise the respective advantages of the two considered approaches. Computationally efficient feature-tracking is used to derive a first estimate of the drift field. The provided vectors serve as initial search position for pattern-matching, that provides accurate drift vectors at each given location including rotation estimate and maximum cross-correlation value. As illustrated in the flowchart in Figure 4, the algorithm consists of five main steps: I Feature tracking,

II Filter, III First guess, IV Pattern matching and V Final drift product.

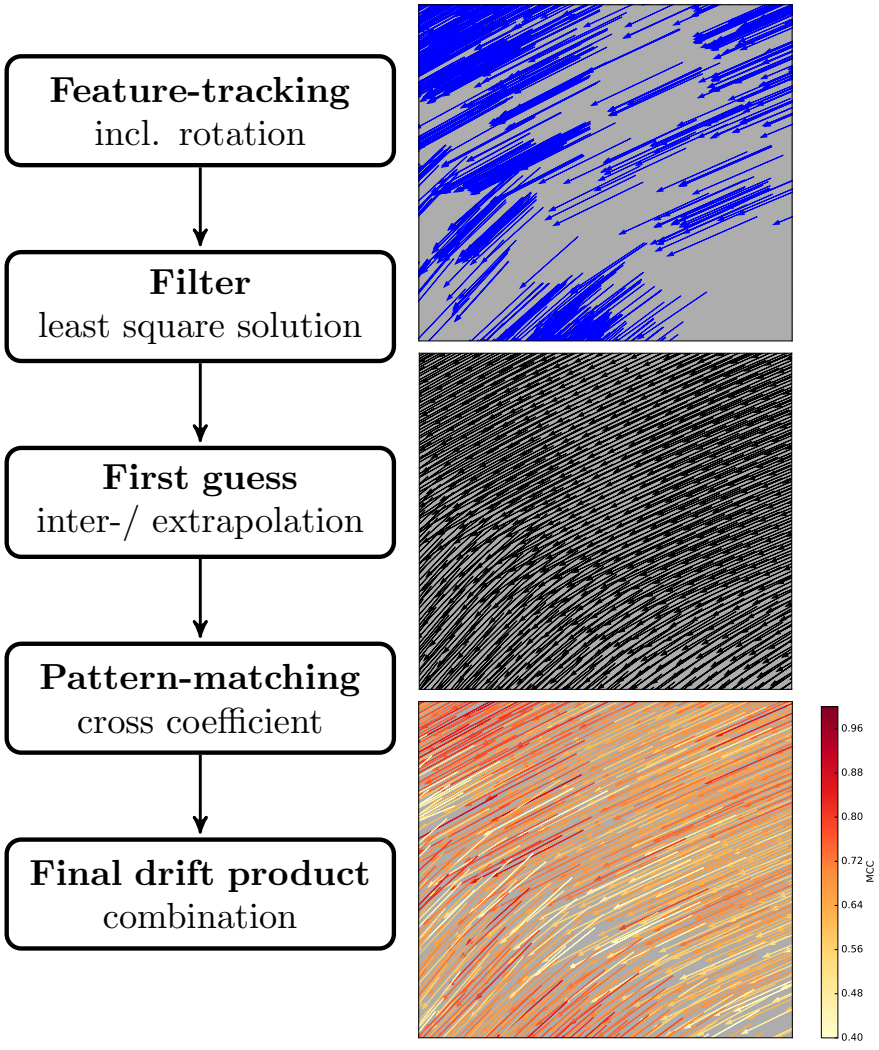

Figure 4. The flowchart on the left depicts the five main steps of the algorithm. The right column illustrates the evolution of the drift results using image pair Fram Strait in HV polarisation and a grid with 4 km spacing. (NB: the part of the image pair that is depicted here is marked with a dashed rectangle in Figure 1.) Blue vectors are derived applying an adjusted version of the feature tracking algorithm from Muckenhuber et al. (2016). Black vectors indicate the initial drift estimate (first guess) based on filtered feature-tracking vectors. The final drift product (yellow to red vectors) are derived from combining the first guess with pattern-matching adjustment and applying a minimum cross-correlation value. ~~In this example, a~~ A total of 4725 vectors have been found on image pair Fram Strait with a MCC value above 0.4 in 4 min.

I Feature-tracking

The feature-tracking algorithm used in this work is an adjusted version from Muckenhuber et al. (2016), who introduced a computationally efficient sea ice drift algorithm for Sentinel-1 based on the ORB (Oriented FAST and Rotated BRIEF) algorithm from Rublee et al. (2011). ORB uses the concept of the FAST keypoint detector (Rosten and Drummond, 2006) to find corners on several resolution levels. The patch around each corner is then described using an modified version of the binary BRIEF descriptor from Calonder et al. (2010). To ensure rotation invariance, the orientation of the patch is calculated using the intensity-weighted centroid. Muckenhuber et al. (2016) applies a Brute Force matcher that compares each feature from the first image to all features in the second image. The comparison of two features is done using the Hamming distance, that represents the number of positions in which the two compared binary feature vectors differ from each other. The best match is accepted if the ratio of the shortest and second shortest Hamming distances is below a certain threshold. Given a suitable threshold (and unique features), the ratio test will discard a high number of false matches, while eliminating only a few correct matches.

Muckenhuber et al. (2016) found a suitable parameter setting for our area and time period of interest, including a Hamming distance threshold of 0.75, a maximum drift filter of 0.5 $\mathrm{m/s}$, a patch size of 34×34 pixels and a resolution pyramid with 7 steps combined with a scaling factor of 1.2. Due to the resolution pyramid, the considered feature area varies from 2.7×2.7 km to 9.8×9.8 km and the resulting drift field represents a resolution mixture between these boundaries.

We adjust the algorithm from Muckenhuber et al. (2016) by applying a logarithmic scaling for the SAR backscatter values σ_0 instead of the previous used linear scaling (Section 3.1). In addition, we extract for each vector the rotation information α, i.e. how much the feature rotates from the first to the second image.

Applying the adjusted feature-tracking algorithm provides a number of un-evenly distributed vectors (e.g. blue vectors in Figure 4) with start positions x_{1f}, y_{1f} on the first image (SAR_1), end positions x_{2f}, y_{2f} on the subsequent image (SAR_2) and corresponding rotation values $\alpha_{raw\,f}$. The index f represents a feature-tracking vector and ranges from 1 to F, with F being the total number of derived feature-tracking vectors. For the sake of computational efficiency, the vectors from all resolution pyramid levels are treated equally.

To avoid zero-crossing issues during the following filter and inter-/extrapolation process (in case the image rotation δ between SAR_1 and SAR_2 is close to 0°), a factor $|180 - \delta|$ is added to the raw rotation values $\alpha_{raw\,f}$ using the following Equation:

$$\alpha_f = \begin{cases} \alpha_{raw\,f} + |180 - \delta| & \text{if } \alpha_{raw\,f} + |180 - \delta| < 360 \\ \alpha_{raw\,f} + |180 - \delta| - 360 & \text{if } \alpha_{raw\,f} + |180 - \delta| > 360 \end{cases} \tag{3}$$

This centres the reasonable rotation values in the proximity of $180°$. After applying the filter and inter-/extrapolation process, the estimated rotation α is corrected by subtracting $|180 - \delta|$.

II Filter

To reduce the impact of potentially erroneous feature-tracking vectors on the following steps, outliers are filtered according to drift and rotation estimates derived from least squares solutions using a third degree polynomial function. Considering a matrix **A**, that contains all end positions x_{2f}, y_{2f} in the following form

$$\mathbf{A} = \begin{pmatrix} 1 & x_{21} & y_{21} & x_{21}^2 & y_{21}^2 & x_{21} * y_{21} & x_{21}^3 & y_{21}^3 \\ 1 & x_{22} & y_{22} & x_{22}^2 & y_{22}^2 & x_{22} * y_{22} & x_{22}^3 & y_{22}^3 \\ \vdots & \vdots & \vdots & \vdots & \vdots & \vdots & \vdots & \vdots \\ 1 & x_{2F} & y_{2F} & x_{2F}^2 & y_{2F}^2 & x_{2F} * y_{2F} & x_{2F}^3 & y_{2F}^3 \end{pmatrix} \tag{4}$$

, we derive three vectors $\boldsymbol{b}_{x_1}$, $\boldsymbol{b}_{y_1}$ and $\boldsymbol{b}_{\alpha}$, that represent the least squares solutions for **A** and $\boldsymbol{x}_1 = (x_{11}, ..., x_{1F})$, $\boldsymbol{y}_1 = (y_{11}, ..., y_{1F})$ and $\alpha = (\alpha_1, ..., \alpha_F)$ respectively. The starting position x_{1f}, y_{1f} and the rotation α_f of each vector can then be simulated using a third degree polynomial function $f(x_{2f}, y_{2f}, \boldsymbol{b})$ depending on the end position x_{2f}, y_{2f} and the corresponding least squares solution $\boldsymbol{b} = (b_0, b_1, b_2, b_3, b_4, b_5, b_6, b_7)$.

$$f(x_{2f}, y_{2f}, \boldsymbol{b}) = b_0 + b_1 x_{2f} + b_2 y_{2f} + b_3 x_{2f}^2 + b_4 y_{2f}^2 + b_5 x_{2f} y_{2f} + b_6 x_{2f}^3 + b_7 y_{2f}^3 \tag{5}$$

If the simulated start position, derived from $f(x_{2f}, y_{2f}, \boldsymbol{b})$, deviates from the feature-tracking start position x_{1f}, y_{1f} by more than 100 pixels, the vector is deleted. The same accounts for rotation outliers. If the simulated rotation deviates from the feature-tracking rotation α_f by more than $60°$, the vector is deleted. We found a third degree polynomial function to be a good compromise between allowing for small to medium scale displacement and rotation discontinuities, and excluding very unlikely vectors, that eventually would disturb the following steps. The parameters for the filter process, i.e. 100 pixels (displacement) and $60°$ (rotation), have been chosen according to visual interpretation using several representative image pairs. Figure 5 illustrates the filter process by depicting the results from image pair Fram Strait.

III First guess

The remaining feature-tracking vectors are used to estimate the drift incl. rotation on the entire first image, i.e. estimated x_2, y_2 and α values are provided for each pixel on SAR_1 (Figure 6). The

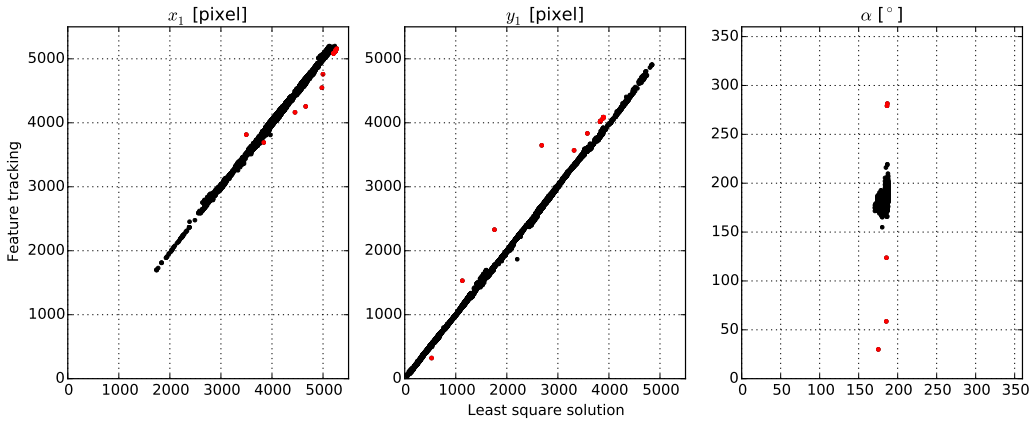

Figure 5. Filter process applied on image pair Fram Strait in HV polarisation. The x-axis represent the simulated start position and rotation, derived from $f(x_{2f}, y_{2f}, \boldsymbol{b})$ and the y-axis represent the feature-tracking start position x_{1f}, y_{1f} and rotation α_f. NB: the image rotation is $\delta = 129.08°$, which means the rotation was adjusted by $50.92°$ (Equation 3). Red points were identified as outliers and deleted.

quality of this 'first guess', however depends on the density of the feature-tracking vector field and the local ice conditions.

Between the feature-tracking vectors, estimated values are constructed by triangulating the input data and performing linear barycentric interpolation on each triangle. That means, the estimated values represent the weighted mean of the three neighbouring feature-tracking values. The interpolated value v_p at any pixel p inside the triangle is given by Equation 6, where v_1, v_2, v_3 represent the feature-tracking values at the corners of the triangle and A_1, A_2, A_3 are the areas of the triangle constructed by p and the two opposite corners, e.g. A_1 is the area between p, and the corners with value v_2 and v_3.

$$v_p = \frac{A_1 v_1 + A_2 v_2 + A_3 v_3}{A_1 + A_2 + A_3} \tag{6}$$

To provide a first guess for the surrounding area, values are estimated based on the least squares solutions using a linear combination of x_1 and y_1. Considering a matrix $\mathbf{C}$, that contains all start positions x_{1f}, y_{1f} in the following form

$$\mathbf{C} = \begin{pmatrix} 1 & x_{11} & y_{11} \\ 1 & x_{12} & y_{12} \\ \vdots & \vdots & \\ 1 & x_{1F} & y_{1F} \end{pmatrix} \tag{7}$$

, we derive three vectors $\boldsymbol{d}_{x_2}$, $\boldsymbol{d}_{y_2}$ and $\boldsymbol{d}_{\alpha}$, that represent the least squares solutions for $\mathbf{C}$ and $\boldsymbol{x}_2 = (x_{21}, ..., x_{2F}), \boldsymbol{y}_2 = (y_{21}, ..., y_{2F})$ and $\alpha = (\alpha_1, ..., \alpha_F)$ respectively. The estimated end position

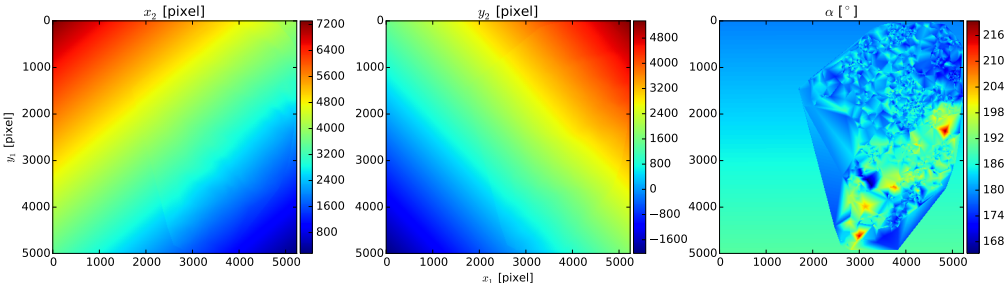

Figure 6. Example of estimated drift and rotation (first guess) based on filtered feature-tracking vectors using image pair Fram Strait in HV polarisation. The three panels show the components x_2, y_2 of the estimated end positions and the estimated rotation α for each pixel on on the coordinate system x_1, y_1 of the first image (SAR_1).

x_2, y_2 and rotation α at any location can then be simulated using the linear function $f(x_1, y_1, \boldsymbol{c})$ depending on the start position x_1, y_1 and the corresponding least squares solution $\boldsymbol{d} = (d_0, d_1, d_2)$.

$$f(x_1, y_1, \boldsymbol{d}) = d_0 + d_1 x_1 + d_2 y_1 \tag{8}$$

As mentioned above, the rotation estimates α are now corrected for the adjustment applied in Equation 3, by subtracting $|180 - \delta|$.

An example for the resulting first guess, i.e. estimated values for x_2, y_2 and α on SAR_1, is shown in Figure 6 (this figure illustrates the matrices that the algorithm considers as first guess) and corresponding vectors are shown in black in Figure 4. Note that rotation α has already been corrected by subtracting $|180 - \delta|$. It includes now both the relative image rotation δ from SAR_1 to SAR_2 and the actual rotation of the feature itself. The introduced algorithm provides also the image rotation δ by projecting the left corners of SAR_2 onto SAR_1 and calculating the angle between the left edges of SAR_1 and SAR_2. The actual rotation of the features can easily be obtained by subtracting δ from α.

IV Pattern-matching

The estimated drift field derived from feature-tracking provides values for x_2, y_2 and α at any location on SAR_1. The representativeness of this estimate however, depends on the distance d to the closest feature-tracking vector. Therefore, small to medium scale adjustments of the estimates are necessary, depending on the distance d (NB: the representativeness also depends on the variability of the surrounding vectors, but for the sake of computational efficiency, we only consider the distance d as representativeness measure). We apply pattern-matching at chosen points of interest to ~~provide more accurate drift vectors and adjust the~~ adjust the drift and rotation estimate at these specific locations.

The used pattern-matching approach is based on the maximisation of the normalised cross-correlation coefficient. Considering a small template t_1 around the point of interest from SAR_1 with size $t_{1s} \times t_{1s}$ and a larger template t_2 around the location x_2, y_2 (defined by the corresponding first guess) from SAR_2 with size $t_{2s} \times t_{2s}$, the normalised cross-correlation matrix **NCC** is defined as (Hollands , 2012):

$$\mathbf{NCC}(x,y) = \frac{\sum_{x',y'}(t_1'(x',y')t_2'(x+x',y+y'))}{\sqrt{\sum_{x',y'} t_1'(x',y')^2 \sum_{x',y'} t_2'(x+x',y+y'))^2}} \tag{9}$$

$$t_1'(x',y') = t_1(x',y') - \frac{1}{t_{1s}^2} \sum_{x'',y''} t_1(x'',y'') \tag{10}$$

$$t_2'(x+x',y+y') = t_2(x+x',y+y') - \frac{1}{t_{1s}^2} \sum_{x'',y''} t_2(x+x'',y+y'') \tag{11}$$

with $t_1(x',y')$ and $t_2(x',y')$ representing the value of t_1 and t_2 at location x',y'. The summations are done over the size of the smaller template, i.e. x', y', x'' and y'' go from 1 to t_{1s}. Template t_1 is moved with step size 1 pixel over template t_2 both in horizontal (x) and vertical (y) direction and the cross-correlation values for each step are stored in the matrix **NCC** with size $(1+t_{s2}-t_{s1}) \times (1+t_{s2}-t_{s1})$. The highest value in the matrix **NCC**, i.e. the the maximum normalised cross-correlation value MCC, represents the location of the best match and the corresponding location adjustment is given by dx and dy.

$$(\frac{1+t_{s2}-t_{s1}}{2} + dx, \frac{1+t_{s2}-t_{s1}}{2} + dy) = \underset{x,y}{argmax}(\mathbf{NCC}(x,y)) \tag{12}$$

To restrict the search area t_{2s} to a circle, we set all values of **NCC** that are further than $t_{2s}/2$ away from the centre position to zero. This limits the distance from the first guess to a constant value, rather than to an arbitrary value depending on the looking angle of the satellite. c To account for rotation adjustment, the matrix **NCC** is calculated several times: template t_1 is rotated around the initially estimated rotation α from $\alpha - \beta$ to $\alpha + \beta$ with step size $\Delta\beta$. The angle β is the maximum additional rotation and represents therefore the rotation restriction. The **NCC** matrix with the highest cross-correlation value MCC is returned.

To illustrate the pattern-matching process, an example, taken from image pair Fram Strait, is shown in Figure 7.

The described process demands the specification of four parameters: t_{1s}, t_{2s}, β and $\Delta\beta$.

The size of the small template $t_{1s} \times t_{1s}$ defines the considered area that is tracked from one image to the next and hence, affects the resolution of the resulting drift product. Sea ice drift might be

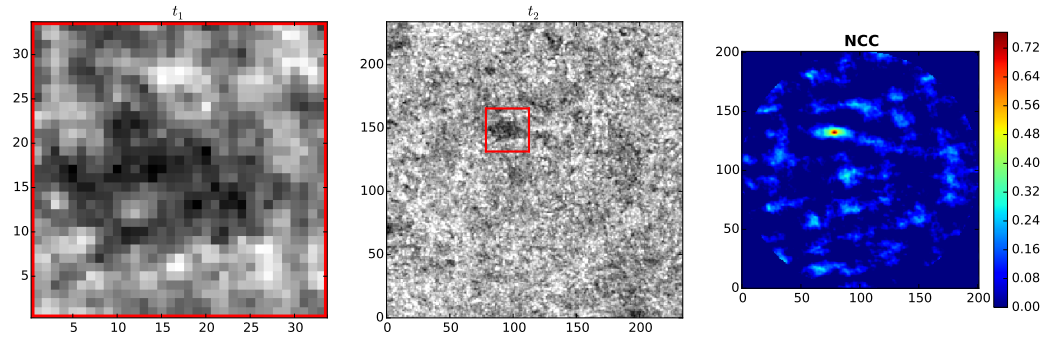

Figure 7. Pattern-matching using initial drift estimate from feature-tracking: The small template t_1 (left) around the point of interest on SAR_1 is rotated from $\alpha-\beta$ to $\alpha+\beta$ and matched with the large template t_2 (middle) from SAR_2, that has its centre at the estimated end position x_2, y_2. The right contour plot shows the normalised cross-correlation matrix **NCC** of the rotation β^* that provided the highest maximum cross-correlation coefficient MCC. The estimated end position x_2, y_2 of this example has to be adjusted by $dx = -21$ pixels, $dy = 32$ pixels to fit with the location of $MCC = 0.71$. Rotation adjustment β^* was found got be 3°. NB: X and Y-axis represent pixel coordinates.

different on different resolution scales. This is particularly an issue in the case of rotation. The feature-tracking vectors provide the first guess and this vector field should represent the same drift resolution as considered by the pattern-matching step. In order to be consistent with the resolution of the feature-tracking step and achieve our goal of a sea ice drift product with a spatial scaling of less than 5 km, we use the size of the feature-tracking patch of the pyramid level with the highest resolution to define the size of t_1. That means, we use $t_{s1} = 34$ pixels (2.7 km).

The size of the larger template $t_{2s} \times t_{2s}$ restricts the search area on SAR_2, i.e. how much the first guess can be adjusted geographically, and the angle β restricts the rotation adjustment of the first guess α. The three parameter t_{2s}, β and $\Delta\beta$ have a strong influence on the computational efficiency of the drift algorithm. Meaning that an increase of t_{2s}, β and a decrease of $\Delta\beta$ increase the computational effort of the pattern-matching step. Based on visual interpretation of several representative image pairs, we found $\Delta\beta = 3°$ to be a good compromise between matching performance and computational efficiency.

Since the ~~uncertainty~~ representativeness of the first guess ~~increases~~ decreases with distance d ~~(Figure 8)~~ to the closest feature-tracking vector (an example to illustrate the distribution of d is shown Figure 8), the search restrictions t_{2s} and β should increase with d. ~~To find useful restrictions for t_{2s} and β, we calculated drift vectors using very high values for t_{2s} and β, i.e. being computationally more demanding than we anticipate, and compared the results with the GPS drift buoy dataset from the N-ICE2015 expedition.~~ Based on the ~~results~~ performed search restriction evaluation (Section 4),

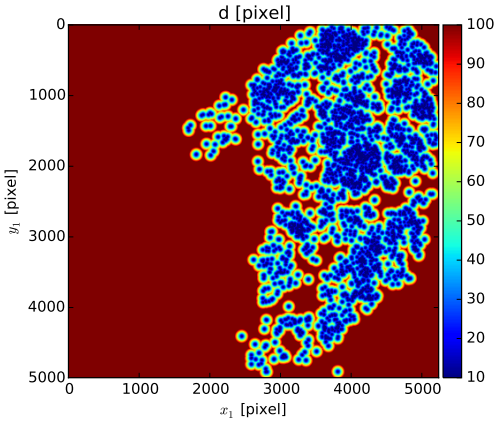

Figure 8. Example to illustrate the distribution of distance d to the closest feature-tracking vector using image pair Fram Strait in HV polarisation. Values outside the range $d_{min} \leq d \leq d_{max}$ are set to $d_{min} = 10$ and $d_{max} = 100$. The points with value d_{min} represent the start positions ~~x_1~~x_{1f}, ~~y_1~~y_{1f} of the feature-tracking vectors on the coordinate system x_1, y_1 of SAR_1. The figure depicts the matrix that the algorithm considers for the distribution of d.

we found the following functions to represent useful restrictions for our area and time period of interest.

$$t_{2s}(d) = t_{1s} + 2d \qquad d_{min} \leq d \leq d_{max} \qquad d \in \mathbb{N} \tag{13}$$

$$\beta(d) = \begin{cases} 9 & \text{if } d < d_{max} \\ 12 & \text{if } d \geq d_{max} \end{cases} \tag{14}$$

The values for d_{min}, d_{max}, β and $\Delta\beta$ can easily be varied in the algorithm to adjust for e.g. different areas, drift conditions or a different compromise between matching performance and computational efficiency.

V Final drift product

In the last step, the small to medium scale displacement adjustments from pattern-matching are added to the estimated first guess derived from feature-tracking. Using buoy comparison, we found that the probability for large displacement errors decreases with increasing MCC value (Section 4). Therefore, vectors that have a MCC value below the threshold MCC_{min} are removed. We found $MCC_{min} = 0.4$ to be a good filter value, but this value can easily be adjusted in the algorithm depending on the sought compromise between amount of vectors and error probability. The algorithm

returns the final drift vectors in longitude, latitude, the corresponding first guess rotation α and the rotation adjustment β in degrees and the maximum cross-correlation value MCC. An example for the final product is depicted with yellow to red coloured vectors in Figure 4. The colour scale refers to the MCC value, indicating the probability for an erroneous vector.

3.3 Comparison with buoy data

Sentinel-1 image pairs have been selected automatically according to position and timing of the GPS buoy data from the N-ICE2015 expedition. Each pair yielded more than 300 drift vectors applying the feature-tracking algorithm from Section 3.2 and had a time difference between the two acquisitions of less than three days. Drift vectors have been calculated with the presented algorithm starting at the buoy GPS position with the least time difference to the acquisition of the first satellite image. The distance D between the calculated end position on the second image and the buoy GPS position with the least time difference to the second satellite acquisition has been calculated using the following equation:

$$D = \sqrt{(u-U)^2 + (v-V)^2} \tag{15}$$

where u and v represent eastward and northward drift components of the displacement vector derived by the algorithm, and U and V the corresponding drift components of the buoy.

4 Results

4.1 Search restrictions evaluation

To find suitable values for restricting the size of the search window t_{2s} and the rotation range defined by β, we calculated drift vectors, that can be compared to the considered GPS buoy dataset, using restrictions that are computationally more demanding than we anticipate for the recommended setting, i.e. $t_{2s} = 434$ pixels and $\beta = 18°$. These values corresponds to a possible pattern-matching adjustment of up to 200 pixels (16 km) and 18° in any direction independent of the distance d to the closest feature-tracking vector.

Based on an automatic search, we found 244 matching Sentinel-1 image pairs (consisting of 111 images), that allowed for comparison with 711 buoy vectors (buoy locations are shown in Figure 9). The distance D (Equation 15) between the buoy location at the time of the second image SAR_2 and the corresponding algorithm result, represents the error estimate for one vector pair. To identify algorithm results that are more likely erroneous, vector pairs with a value D above 1000 m are marked with red dots in Figure 10 and Figure 11. Vector pairs with $D < 1000$ m are plotted with black dots.

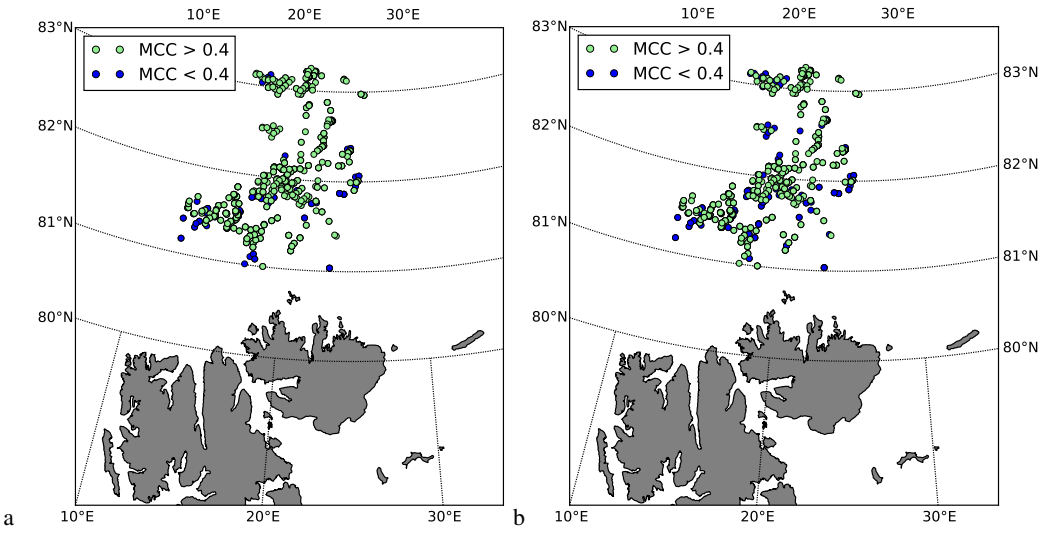

Figure 9. Considered buoy locations from the N-ICE2015 expedition that were used for comparison with algorithm results. Green and blue colour indicates start locations (on SAR_1) to which the algorithm provided vectors with a MCC value above and below 0.4 using (a) HV and (b) HH polarisation.

Figure 10 and Figure 11 show the resulting pattern-matching adjustment of location (dx, dy) and rotation ($d\beta$) using the computationally demanding restrictions. The values are plotted against distance d to the next feature tracking vector in order to identify the dependence of the parameters on d. The blue lines in Figure 10 and Figure 11 indicate the recommended restrictions. This represents a compromise between computational efficiency and allowing the algorithm to adjust the first guess as much as needed for our time period and area of interest. The corresponding functions for $t_{2s}(d)$ and $\beta(d)$ are given in Equation 13 and Equation 14 and the recommended boundary values for distance d are $d_{min} = 10$ and $d_{max} = 100$.

4.2 ~~Validation~~Performance assessment

Using the recommended search restrictions from above, the algorithm has been ~~validated against~~ compared to the N-ICE2015 GPS buoy data set (Figure 9) to assess the potential performance after finding suitable search restrictions for the area and time period of interest. The automatic search provided 246 image pairs (consisting of 111 images) and 746 vectors for comparison for the considered time period (15^{th} January to 22^{nd} April) and area (80.5° N to 83.5° N and 12° E to 27° E). NB: this is a higher number of vectors than found for the evaluation of the search restrictions, since the used search windows t_2 are smaller and vectors closer to the SAR edge may be included.

The results of the conducted ~~validation~~ performance assessment are shown in Figure 12. We found that the probability for a large D value (representative for the error) decreases with increasing maximum cross-correlation value MCC. Therefore we suggest to exclude matches with a MCC value

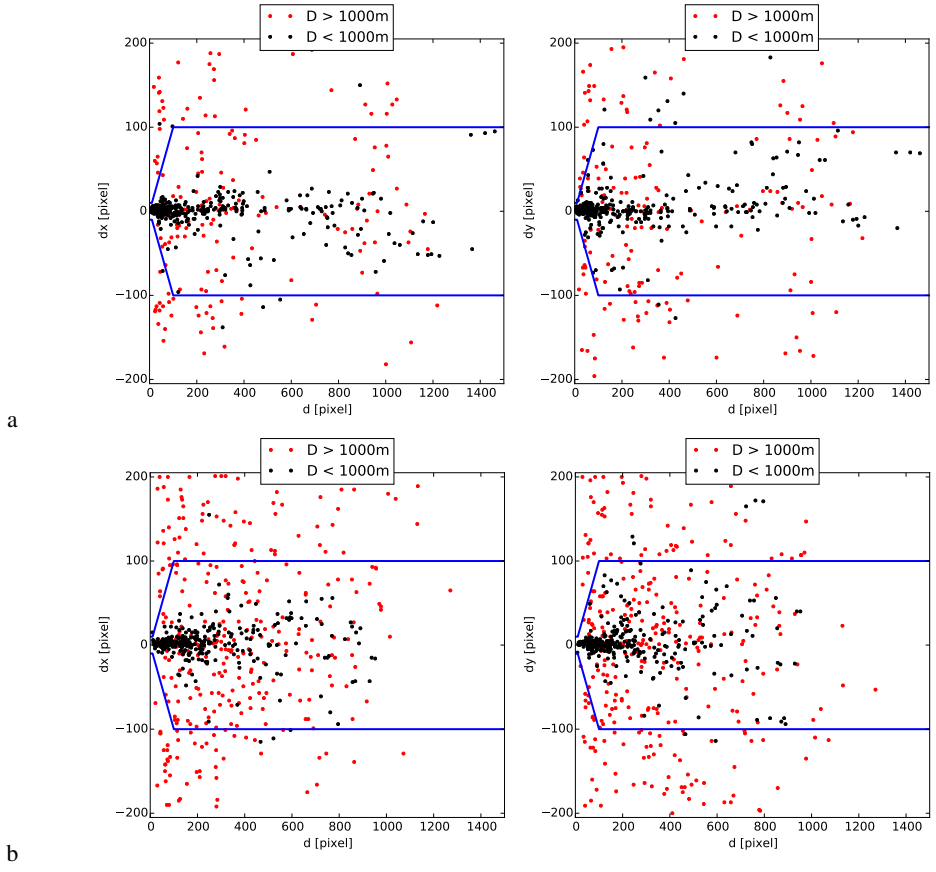

Figure 10. Pattern-matching location adjustment dx and dy in x and y direction versus distance d to closest feature tracking vector using (a) HV and (b) HH polarisation. D represents the difference between buoy GPS position and algorithm result. The blue lines indicate the recommended setting for t_{2s} (Equation 13) with $d_{min} = 10$ and $d_{max} = 100$.

below a certain threshold MCC_{min}. This option is embedded into the algorithm, but can easily be adjusted or turned off by setting $MCC_{min} = 0$. Based on the findings shown in Figure 12, we recommend a cross-correlation coefficient threshold $MCC_{min} = 0.4$ for our time period and area of interest. Using the suggested threshold reduces the number of vector pairs from 746 to 588 for the HV channel and to 478 for the HH channel.

The conducted ~~validation~~ performance assessment also reveals a logarithmic normal distribution of the distance D (Equation 15) that can be expressed by the following probability density function (solid red line in Figure 12):

$$lnN(D;\mu,\sigma) = \frac{1}{\sigma D\sqrt{2\pi}} e^{-\frac{(\ln D-\mu)^2}{2\sigma^2}} \tag{16}$$

with μ and σ being the mean and standard deviation of the variable's natural logarithm. We found the mean and variance of the distribution lnN to be $\mu = 5.866$ and $\sigma^2 = 1.602$ for HV polarisation

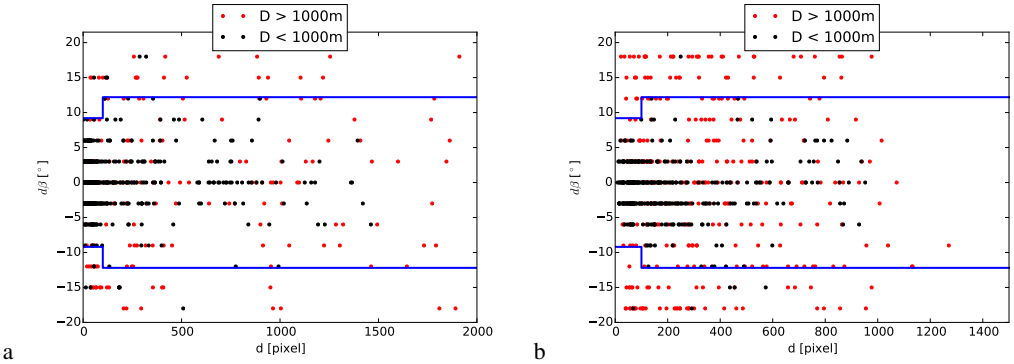

Figure 11. Pattern-matching rotation adjustment $d\beta$ versus distance d to closest feature tracking vector using (a) HV and (b) HH polarisation. D represents the difference between buoy GPS position and algorithm result. The blue lines indicate the recommended setting for β (Equation 14) with $d_{min} = 10$ and $d_{max} = 100$.

Table 1. Recommended parameter setting for sea ice drift retrieval from Sentinel-1 using the presented algorithm.

Parameter	Meaning	Recommended setting
$[\sigma^0_{\min}, \sigma^0_{\max}]$ (HH)	Brightness boundaries for HH channel	[-25 dB, -10.97 dB]
$[\sigma^0_{\min}, \sigma^0_{\max}]$ (HV)	Brightness boundaries for HV channel	[-32.5 dB, -18.86 dB]
t_{1s}	Size of template t_1	34 pixels (2.7 km)
$[d_{min}, d_{max}]$	Boundaries for distance d	[10 pixels, 100 pixels]
MCC_{min}	Threshold for cross-correlation	0.4
$\Delta\beta$	Rotation angle increment	3°

and $\mu = 6.284$ and $\sigma^2 = 2.731$ for HH polarisation (solid red lines in Figure 12). The medians of the logarithmic normal distribution are $e^{\mu} = 352.9\,m$ for HV polarisation and $e^{\mu} = 535.7\,m$ for HH polarisation (dashed red lines in Figure 12).

4.3 Recommended parameter setting

Based on the restriction evaluation, our experience with the algorithm behaviour, and considering a good compromise between computational efficiency and high quality of the resulting vector field, we recommend the parameter setting shown in Table 1 for our area and time period of interest. The corresponding recommended values for $t_{2s}(d)$ and $\beta(d)$ are given in Equation 13 and Equation 14.

4.4 Computational efficiency

The processing time depends on the parameter setting and the chosen vector distribution. Using the recommended parameter setting from Table 1, allows high-resolution sea ice drift retrieval from a Sentinel-1 image pair within a few minutes. Figure 4 depicts calculated ice drift vectors for the

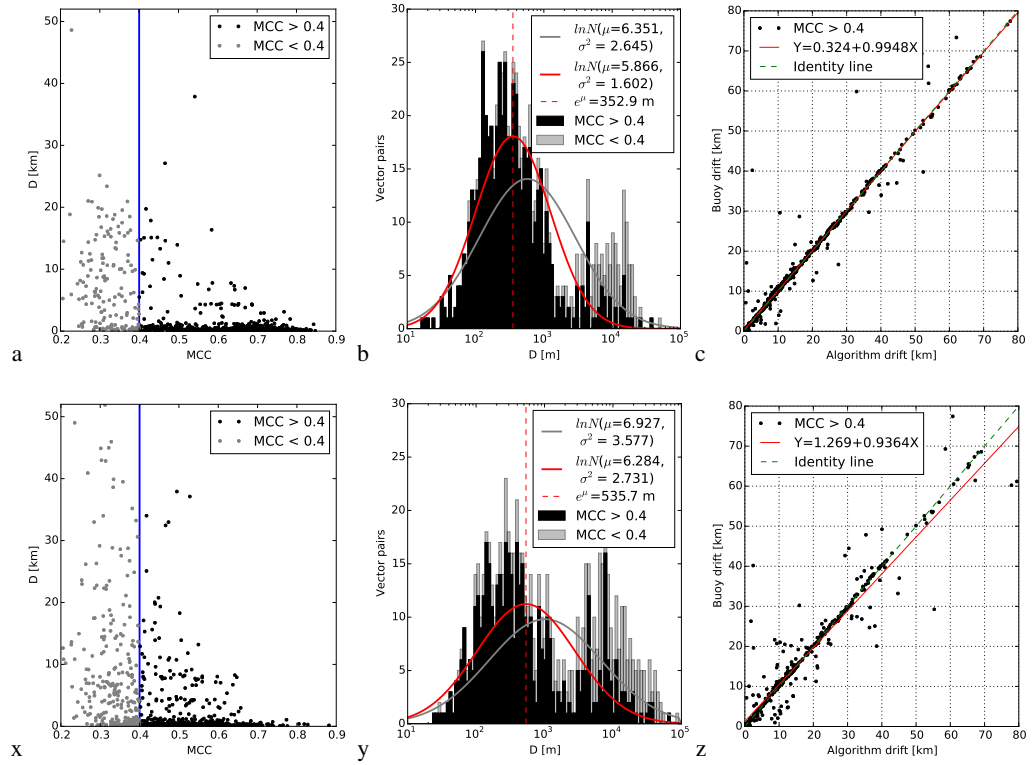

Figure 12. Calculated ice drift using recommended search restrictions compared to buoy GPS data using (a,b,c) HV and (x,y,z) HH polarisation. Light grey represents vectors with maximum cross-correlation values $MCC < 0.4$ and results after using the suggested threshold $MCC_{min} = 0.4$ are shown in black. (a,x) MCC values against distance D (Equation 15) between algorithm and buoy end position. The blue line indicates the recommended setting for $MCC_{min} = 0.4$. (b,y) Logarithmic histogram of distance D with 100 bins between 10 m and 10^5 m including two logarithmic normal distributions that were fitted to all results (grey) and to the filtered results with $MCC > 0.4$ (solid red line). (c,z) Comparison of drift distance derived from algorithm against buoy displacement for the filtered results with $MCC > 0.4$.

image pair Fram Strait on a grid with 4 km (50 pixels) spacing. The corresponding processing times are shown in Table 2. The calculations have been done using a MacBook Pro from early 2013 with a 2.7 GHz Intel Core i7 processor and 8 GB 1600 MHz DDR3 memory. The total processing time for 4725 vectors with a normalised cross-correlation value above 0.4, is about 4 minutes. This can be considered a representative value for an image pair with large overlap, good coverage with feature-tracking vectors and 4 km grid spacing.

The initial process in Table 2 'Create Nansat objects from Sentinel-1 image pair and read matrixes' takes the same amount of computational effort for all image pairs consisting of Sentinel-1 images with 400x400 km coverage.

Table 2. Processing time for sea ice drift retrieval from image pair Fram Strait on a grid with 4 km (50 pixels) spacing using HV polarisation (Figure 4). Representative for an image with large overlap and good coverage with feature-tracking vectors.

Process	Time [s]
Create Nansat objects from Sentinel-1 image pair and read matrixes	70
I Feature-tracking	66
II Pattern-matching and III Combination	107
$\sum$ Sea ice drift retrieval	243

The process 'I Feature-tracking' depends on the setting of the feature-tracking algorithm and varies strongly with the chosen number of features. Using the recommended setting from Muckenhuber et al. (2016), that includes the number of features to be 100000, the presented computational effort can be considered representative for all image pairs, independent of chosen points of interest and overlap of the SAR scenes.

The last process 'II Pattern-matching and III Combination' however, depends on the considered image pair and the chosen drift resolution. The computational effort is proportional to the number of chosen points of interest. Given a evenly distributed grid of points of interest, the computational effort increases with overlapping area of the SAR scenes, since pattern-matching adjustments are only calculated in the overlapping area. The effort potentially decreases with a higher number of well distributed feature-tracking vectors, since the size of the search windows t_2 (and slightly the range of the angle β) increases with distance d to the closest feature-tracking vector.

5 Discussion and outlook

To estimate the ~~accuracy~~ potential performance of the introduced algorithm ~~,~~ for given image pairs, given ice conditions, given region and given time, we compared drift results from 246 Sentinel-1 image pairs with corresponding GPS positions from the N-ICE2015 buoy data set. We found a logarithmic error distribution with a median at 352.9 m for HV and 535.7 m for HH (Figure 12). The derived error values represent a combination of the following error sources:

- Timing: Buoy GPS data were collected every 1-3 hours and the timing does not necessarily match with the satellite acquisition time.
- Resolution: The algorithm returns the drift of a pattern (recommended size = 34 pixels, see Table 1), whereas the buoy measures the drift at a single location.

- Conditions: The ice conditions around the buoy is not known well enough to exclude the possibility that the buoy is floating in a lead. In this case, the buoy trajectory could represent a drift along the lead rather then the drift of the surrounding sea ice.
- actual error of the algorithm.

A main advantage of the combined algorithm compared to simple feature-tracking, is the user defined positioning of the drift vectors. The current algorithm setup allows the user to choose whether the drift vectors should be positioned at certain points of interest or on a regular grid with adjustable spacing. Constricting the pattern-matching process to the area of interest minimises the computational effort according to the individual needs.

The recommended parameters shown in Table 1 are not meant as a fixed setting, but should rather give a suggestion and guideline to estimate the expected results and the corresponding computational effort. The parameters can easily be varied in the algorithm setup and should be chosen according to availability of computational power, needed resolution, area of interest and expected ice conditions (e.g. strong rotation).

The presented combination of feature-tracking and pattern-matching can be applied to any other application that aims to derive displacement vectors computationally efficient from two consecutive images. The only restriction is that images need to depict edges, that can be recognised as keypoints for the feature-tracking algorithm, and the conversion into intensity values i (Equation 2) needs to be adjusted according to the image type.

The remote sensing group at NERSC is currently developing a new pre-processing step to remove thermal noise on HV images over ocean and sea ice. First tests have shown a significant improvement of the sea ice drift results using this pre-processing step before applying the presented algorithm. This is ongoing work and will be included into a future version of the algorithm.

The European Space Agency is also in the process of improving their thermal noise removal for Sentinel-1 imagery. Noise removal in range direction is driven by a function that takes measured noise power into account. Until now, noise measurements are done at the start of each data acquisition, i.e. every 10-20 minutes, and a linear interpolation is performed to provide noise values every 3 seconds. The distribution of noise measurements showed a bimodal shape and it was recently discovered that lower values are related to noise over ocean while higher values are related to noise over land. This means, that Sentinel-1 is able to sense the difference of the earth surface brightness temperature similar to a passive radiometer. When the data acquisition includes a transition from ocean to land or vice versa, the linear interpolation fails to track the noise variation. The successors of Sentinel-1A/B are planned to include more frequent noise measurements. Until then, ESA wants to use the 8-10 echoes after the burst that are recorded while the transmitted pulse is still travelling and the instrument is measuring the noise. This will provide noise measurements every 0.9 seconds and allows to track the noise variations in more detail. In addition, ESA is planning to introduce a change in the data format during 2017 that shall remove the noise shaping in azimuth. These ef-

forts are expected to improve the performance of the presented algorithm significantly (Personal Communication with Nuno Miranda, January 2017).

Having a computationally efficient algorithm with adjustable vector positioning allows not only to provide near-real time operational drift data, but also the investigation of sea ice drift over large areas and long time periods. Our next step is to embed the algorithm into a super-computing facility to further test the performance in different regions, time periods and ice conditions and evaluate and combine the results of different polarisation modes. The goal is to deliver large ice drift datasets and open-source operational sea ice drift products with a spatial resolution of less than 5 km.

This work is linked to the question how to combine the different timings of the individual image pairs in a most useful way. Having more frequent satellite acquisitions, as we get with the Sentinel-1 satellite constellation, enables to derive displacements for shorter time gaps and the calculated vectors will reveal more details e.g. rotational motion due to tides. As part of a scientific cruise with KV-Svalbard in July 2016, we deployed three GPS trackers on loose ice floes and pack-ice in Fram Strait. The trackers send their position every 5-30 min to deliver drift information with high temporal resolution. This efforts shall help to gain a better understanding of short-term drift variability and by comparison with calculated sea ice drift, we will investigate how displacement vectors from subsequent satellite images relate to sea ice displacements with higher temporal resolution.

The focus of this paper in terms of polarisation was put on the HV channel, since this polarisation provides on average four times more ~~feature tracking vectors~~ feature-tracking vectors (using our feature-tracking approach) than HH and therefore delivers a finer initial drift for the first guess. We found our area of interest well covered with HV images, but other areas in the Arctic and Antarctic are currently only monitored in HH polarisation. Considering the four representative feature-tracking image pairs from Muckenhuber et al. (2016), the ~~the~~ relatively best HH polarisation performance (i.e. most vectors from HH, while at the same time fewest vectors from HV) was provided by the image pair that had the least time difference, i.e. 8 h, compared to 31 h, 33 h and 48 h. Therefore, we assume that the HV polarisation provides more corner features that are better preserved over time. And more consistent features could potentially also favour the performance of the pattern-matching step, but this is only an assumption and has not been tested yet. Another argument is that the presented feature-tracking approach identifies and matches corners, which represent linear features. The linear features on HH images are more sensitive to changes in incidence angle, orbit and ice conditions than the linear features on HV images. This could explain the better feature-tracking performance of the HV channel. However, pattern-matching is less affected by changing linear features and more sensitive to areal pattern changes. This could potentially mean that the HH channel performs better than HV when it comes to pattern-matching. However, at this point, these are just assumptions and will be addressed in more detail in our future work.

Utilising the advantage of dual polarisation (HH+HV) is certainly possible with the presented algorithm, but increases the computational effort. A simple approach is to combine the feature track-

ing vectors derived from HH and HV and produce a combined first-guess. Pattern-matching can be performed based on this combined first-guess for both HH and HV individually and the results can be compared and eventually merged into a single drift product. Having two drift estimates for the same position, from HH and HV pattern-matching respectively, would also allow to disregard vectors that disagree significantly. However, this option would increase the computational effort by two, meaning that the presented Fram Strait example would need about 8 min processing time.

After implementing the presented algorithm into a super-computing facility, we aim to test and compare the respective performance of HV, HH and HH+HV on large datasets to identify the respective advantages.

The current setting of the feature-tracking algorithm applies a maximum drift filter of 0.5 m/s. We found this to be a reasonable value for our time period and area of interest. However, when considering extreme drift situations in Fram Strait and a short time interval between image acquisitions, this threshold should be adjusted.

As mentioned above, we deployed three GPS tracker in Fram Strait and they recorded their positions with a temporal resolution of 5-30 min between 8^{th} July until 9^{th} September 2016 in an area covering 75° N to 80° N and 4° W to 14° W. Considering the displacements with 30 min interval, we found velocities above 0.5 m/s on a few occasions, when the tidal motion adds to an exceptionally fast ice drift.

The GPS data from the hovercraft expedition FRAM2014-2015 (https://sabvabaa.nersc.no), that was collected with a temporal resolution of 10 s between 31^{st} August 2014 until 6^{th} July 2015, did not reveal a single 30 min interval during which the hovercraft was moved by ice drift more than 0.45 m/s. The hovercraft expedition started at 280 km south from the North Pole towards the Siberian coast, crossed the Arctic Ocean towards Greenland and was picked up in the north-western part of Fram Strait.

In case the estimated drift from feature-tracking reaches velocities close to 0.5 m/s, the pattern-matching step might add an additional degree of freedom of up to 8 km, which could eventually lead to a higher drift result than 0.5 m/s, depending on the time interval between the acquisitions. The smaller the time difference, the larger is the potentially added velocity. In order to be consistent when combining the drift information from several image pairs with different timings, one should apply a maximum drift filter on the final drift product of the presented algorithm that has the same maximum velocity as the feature-tracking filter. The corresponding function is implemented in the distributed open-source algorithm. As an alternative, one could adjust the search window according to the time span. However, this would add additional complexity to both the algorithm and the parameter evaluation and needs more research on how the search window should be adjusted depending on the time span. For the sake of computational efficiency, we suggest the simple approach to remove final drift vectors above the maximum speed.

Appendix A: Open-source distribution

The presented sea ice drift retrieval method is based on open-source satellite data and software to ensure free application and easy distribution. Sentinel-1 SAR images are distributed by ESA for free within a few hours of acquisition under https://scihub.esa.int/dhus/. The algorithm is programmed in Python (source code: https://www.python.org) and makes use of the open-source libraries Nansat, openCV and SciPy. Nansat is a Python toolbox for processing 2-D satellite Earth observation data (source code: https://github.com/nansencenter/nansat). OpenCV (Open Source Computer Vision) is a computer vision and machine learning software library and can be downloaded under http://opencv.org. SciPy (source code: https://www.scipy.org) is a Python-based ecosystem of software for mathematics, science, and engineering. The presented sea ice drift algorithm, including an application example, is distributed as open-source software ~~under .~~ as supplement to this manuscript.

Author contributions. Stefan Muckenhuber designed the algorithm and the experiments, performed the data analysis and interpretation of the results and wrote the manuscript. Stein Sandven critically revised the work and gave important feedback for improvement. Stefan Muckenhuber and Stein Sandven approved the final version for publication.

Acknowledgements. This research was supported by the Norwegian Research Council project IceMotion (High resolution sea-ice motion from Synthetic Aperture Radar using pattern tracking and Doppler shift, project number 239998/F50). We thank Polona Itkin and Gunnar Spreen for providing us the buoy GPS data that were collected as part of the N-ICE2015 project with support by the Norwegian Polar Institute's Centre for Ice, Climate and Ecosystems (ICE) and its partner institutes. The used satellite data were provided by the European Space Agency. We thank Nuno Miranda for information on ESA's de-noising efforts for Sentinel-1.

References

Berg, A. and Eriksson L.E.B.: Investigation of a Hybrid Algorithm for Sea Ice Drift Measurements Using Synthetic Aperture Radar Images IEEE Transactions on Geoscience and Remote Sensing, Vol. 52, No. 8, 5023–5033, 2014.

Calonder, M., Lepetit, V., Strecha, C., and Fua, P.: BRIEF: Binary Robust Independent Elementary Features, CVLab, EPFL, Lausanne, Switzerland, 2010.

ESA: Sentinel-1 ESA's Radar Observatory Mission for GMES Operational Services, ESA Communications, SP-1322/1, ISBN: 978-92-9221-418-0, ISSN: 0379-6566, 2012.

Hollands, T.: Motion tracking of sea ice with SAR satellite data, dissertaiton, Section 2: Estimation of motion from images, University Bremen, 2012.

Hollands, T. and Dierking, W.: Performance of a multiscale correlation algorithm for the estimation of sea-ice drift from SAR images: initial results, Ann. Glaciol., 52, 311–317, 2011.

IPCC – Intergovernmental Panel on Climate Change: Climate Change 2013: The Physical Science Basis, Fifth Assessment Report, AR5, 317–382, 323–335, 2013.

Komarov, A.S., and Barber, D.G.: Sea Ice Motion Tracking From Sequential Dual-Polarization RADARSAT-2 Images, IEEE Transactions on Geoscience and Remote Sensing, Vol. 52(1), No. 1, 121–136, doi: 10.1109/TGRS.2012.2236845, 2014.

Korosov A.A., Hansen W.M., Dagestad F.K., Yamakawa A., Vines A., Riechert A.: Nansat: a Scientist-Orientated Python Package for Geospatial Data Processing, Journal of Open Research Software, 4: e39, DOI: http:// dx.doi.org/10.5334/jors.120, 2016

Kwok, R., Curlander J.C., McConnell R., and Pang S.: An Ice Motion Tracking System at the Alaska SAR Facility, IEEE Journal of Oceanic Engineering, Vol. 15, No. 1, 44–54, 1990.

Muckenhuber S., Korosov A.A., and Sandven S. (2016): Open-source feature-tracking algorithm for sea ice drift retrieval from Sentinel-1 SAR imagery, The Cryosphere, 10, 913-925, doi:10.5194/tc-10-913-2016, 2016

Nansen, F.: The Oceanography of the North Polar Basin. Scientific Results, Vol. 3, 9, Longman Green and Co., Kristinania, Norway, 1902.

Pedersen, L.T., Saldo, R. and Fenger-Nielsen, R.: Sentinel-1 results: Sea ice operational monitoring, Geoscience and Remote Sensing Symposium (IGARSS), IEEE International, 2828–2831, doi=10.1109/IGARSS.2015.7326403, 2015

Rampal, P., Weiss, J., Marsan, D. and Bourgoin M.: Arctic sea ice velocity field: General circulation and turbulent-like fluctuations, Journal of Geophysical Research: Oceans, Vol. 114, Nr. C10014, doi=10.1029/2008JC005227, 2009.

Rampal, P., Weiss, J. and Marsan, D.: Positive trend in the mean speed and deformation rate of Arctic sea ice 1979–2007, Journal of Geophysical Research: Oceans, Vol. 114, Nr. C5013, doi=10.1029/2008JC005066, 2009b.

Rosten, E. and Drummond, T.: Machine learning for high-speed corner detection, in European Conference on Computer Vision, ISBN 978-3-540-33833-8, 430–443, doi: 10.100711744023_34, 2006.

Rublee, E., Rabaud, V., Konolige, K., and Bradski, G.: ORB: an efficient alternative to SIFT or SURF, IEEE I. Conf. Comp. Vis. (ICCV), ISBN: 978-1-4577-1101-5, 2564–2571, doi: 10.1109ICCV.2011.6126544, 6–13 Nov, 2011.

Spreen, G. and Itkin, P.: N-ICE2015 buoy data, Norwegian Polar Institute, https://data.npolar.no/dataset/6ed9a8ca-95b0-43be-bedf-8176bf56da80, 2015.

Thomas, M., Geiger, C. A., and Kambhamettu, C.: High resolution (400 m) motion characterization of sea ice using ERS-1 SAR imagery, Cold Reg. Sci. Technol., 52, 207–223, 2008.

Thorndike, A. S. and Colony, R.: Sea ice motion in response to geostrophic winds, Journal of Geophysical Research: Oceans, Vol. 87, Nr. C8, 5845–5852, doi=10.1029/JC087iC08p05845, 1982.

Widell, K., Østerhus, S. and Gammelsrød, T.: Sea ice velocity in the Fram Strait monitored by moored instruments, Geophysical Research Letters, Vol. 30, Nr. 19, doi=10.1029/2003GL018119, 2003.